Journal of Biomedical Optics

SPIEDigitalLibrary.org/jbo

Spectral dependence of absorption sensitivity on concentration of oxygenated hemoglobin: pulse oximetry implications

Marija Strojnik
Gonzalo Paez

SPIE

Spectral dependence of absorption sensitivity on concentration of oxygenated hemoglobin: pulse oximetry implications

Marija Strojnik and Gonzalo Paez
Centro de Investigaciones en Optica, Apdo Postal 1-948, C. P. 37000 Leon, Guanajuato, Mexico

Abstract. The sensitivity analysis indicates that the effective absorption coefficient is most sensitive to the concentration of oxygenated hemoglobin in spectral bands centered at 700 and 960 nm. We find that the highest temporal modulation due to heart function for a thick sample, like an arm, is at 940 nm, a significant shift from 710 nm measured for a finger. The most favorable spectral region for a thick transmission sample, such as a forearm, is the domain defined by intervals [900 nm $\leq \lambda_1 \leq$ 1000 nm] and [650 nm $\leq \lambda_2 \leq$ 720 nm]. We evaluated five near-infrared light-emitting diodes (LEDs) for their potential applications in oximetry. The LED with peak emission at 930 nm emits well in this spectral region. Here the temporal noise is low, and the effective absorption coefficient is strongly dependent on the concentration of the oxygenated hemoglobin. High-quality saturation results are obtained through the forearm during a short measurement (30 s). [DOI: 10.1117/1.JBO.18.10.108001]

Keywords: oximetry; pulse oximetry; spectroscopy; sensitivity; medical optics; human functions as temporal noise; near-infrared; hemoglobin; oxygenation; oxygen saturation.

Paper 130389R received Jun. 4, 2013; revised manuscript received Jul. 23, 2013; accepted for publication Aug. 1, 2013; published online Oct. 2, 2013.

1 Introduction

The relatively low radiation attenuation within the biological tissues in the spectral interval [650 to 1050 nm] makes this band of great interest for patient monitoring.[1–9] The advantage of optical techniques is that they are practical even for immobilized, unresponsive patients. Possibly, their greatest disadvantage is the introduction of the temporal component of signal due to the functioning of living organs producing effects that may be quite irregular, unpredictable, and random.[10–15] Collection of spectroscopic data on a living specimen is hindered by appreciably more noise than that on a material with comparable composition, such as phantoms, or *in vitro* tissue.[16,17] Temporal noise, when properly understood and characterized, may be decreased by appropriate selection of experimental parameters.[18,19]

Oximetry is a noninvasive technique to monitor oxygen saturation due to respiratory or chronic obstructive pulmonary diseases, including acute asthma, and their side effects,[20,21] and to detect the onset of hypoxia.[22] The hemoglobin is responsible for bringing oxygen to the tissue. The absorption of oxy-hemoglobin (HbO_2) is different from that of deoxy-hemoglobin (Hb) at wavelengths within the therapeutic window. Carboxy-hemoglobin and methemoglobin detection has recently become available.[23]

Pulse oximeters are used to determine oxygen saturation in arterial hemoglobin and pulse rate monitoring to assess additional vital signs.[24] The spectral transmission function measured on a live subject at rest has a temporally modulated component due to heart pumping and breathing. For a healthy human at rest, this phenomenon is generally ascribed to the volume change in the arterial blood.[25–30]

In recent years, pulse oximeter technology has advanced significantly to monitor patients during challenging conditions such as poor-transmitted signal, high levels of noise, presence of movement artifacts, or during significant hypoxic episodes.[31,32] The photoplethysmographic waveform in infrared (IR) is used to determine the pulse rate.[33–35] Pulse oximetry is used in early detection and status assessment for chronic arterial insufficiency in extremities.[36] Applications of oximetry to monitor thick samples and with unresponsive patients have been reported.[37–41]

In the last 10 years, pulse oximetry has undergone significant development[42] in noncontact monitoring,[43–45] in imaging,[46–48] and finally in incorporating diffuse imaging and backscattering in remote systems.[49–51]

An alive human is a source of much noise upon breathing, talking, beating of the heart, and physiological and psychological states, in addition to the actual illness that is being assessed. Several established experimental techniques may be used to ameliorate the effects of temporal noise. This includes signal processing of the sought-after quantity, the preferred method in the statistical analysis of data processing for random noise.[52] The most compact illumination sources in NIR are laser diodes and light emission diodes (LED). The relatively long time dedicated to determine the oxygen saturation value, combined with low uncertainty of actual radiometric measurements, prompted us to propose the standard deviation as a figure-of-merit for the optimal wavelength selection.[53]

Next, we comment on the terminology employed in this article. We use the term transillumination to denote the phenomenon that radiation is transmitted through partially scattering and partially transmitting media and detected on the other side, especially when it does not follow a straight path.

Address all correspondence to: Marija Strojnik, Centro de Investigaciones en Optica, Apdo Postal 1-948, C. P. 37000 Leon, Guanajuato, Mexico. Tel: +477 441 4200; Fax: +477 441 4209; E-mail: mstrojnikp@aol.com

Transmission refers to the radiation that follows a straight path without slowing down, except due to the effects of the index of refraction. Otherwise, we adhere to the traditional radiometric terminology.[54]

The objective of the current work is the development of a versatile pulse oximeter that has an improved signal-to-noise ratio, is insensitive to temporal noise, and may be applied to thick, multitissue parts of body, such as an arm or a cranium, during a short measurement. In this context, "short" means less than a minute, often 30 s, deviating from the current practice of continuous monitoring. This improvement also serves as the basis for noncontact plethysmographic monitoring. We perform sensitivity analysis to identify wavelength bands, where the signal is most susceptible to changes in the oxygenated hemoglobin concentration.

In the next section, we introduce the concept of functional oxygen saturation and its effects on the effective absorption coefficients within the therapeutic window. In Sec. 3, we examine the temporal modulation in the radiometric signal. We measure it for different monitoring locations. We describe the sensitivity analysis on the effective absorption coefficient and its dependence on the HbO_2 concentration. Several relatively wide spectral band LEDs are evaluated for potential use as illumination sources, as described in Sec. 4. We propose one with suitable radiometric characteristics in the spectral interval, where thick biological samples exhibit low noise. The findings are summarized in the last section: the duration of the pulse oximetry measurement may be significantly decreased.

2 Oxygen Saturation Determination

The specific absorption coefficients of oxygenated (HbO_2) and deoxygenated hemoglobin (Hb) have distinct spectral dependence, as included in Fig. 1 (see also Ref. 1). The difference between these coefficients allows for the quantification of each constituent, forming the basis of oximetry.

Two wavelengths, as a minimum, are chosen to determine the oxygen saturation. The profiles of the specific absorption coefficients are frequently analyzed, in order to select the most appropriate monitoring wavelengths. The choice for the wavelength pair often includes a narrow band at 660 nm to detect the absorption peak of Hb and one at 940 nm for the peak of HbO_2.

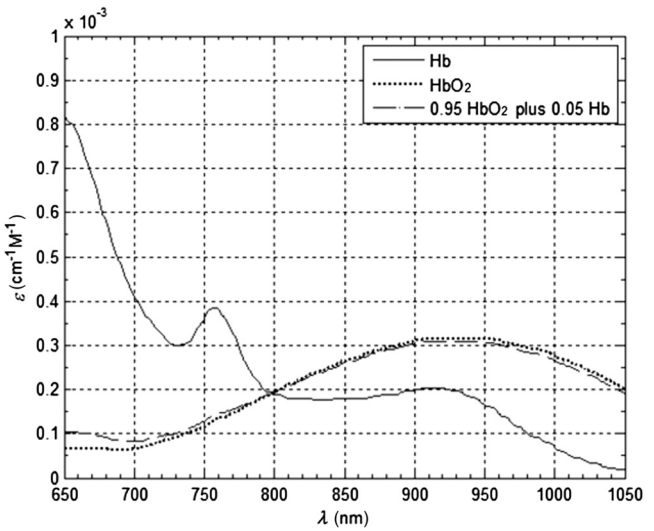

Fig. 1 Specific absorption coefficients of oxy- and deoxy-hemoglobin as a function of wavelength in the therapeutic window [650 to 1050 nm].

We perform sensitivity analysis to determine two wavelength bands, where the specific absorption coefficient is most sensitive to the change in the concentration of the oxygenated hemoglobin. We propose an alternate wavelength selection criterion that is based on the functional range of the saturation from 0.8 to 1.0 with the critical value of 0.9 ± 0.1.

2.1 *Functional Limits of Oxygen Saturation*

In a clinical situation, a patient is delivered with oxygen when the measured saturation value falls below 0.89. The values between 0.90 and 0.95 are encouraging in the case of a postoperative patient who is learning to breathe effectively on his or her own. As it determines critical intervention in the patient care, we refer to oxygen saturation of 0.9 as a critical saturation. Thus, the most accurate and reliable saturation measurement must be performed at ~0.9.

In Fig. 1, the HbO_2 curve by itself could be interpreted as the absorption coefficient for the special case when the blood is 100% oxygenated. Similarly, the Hb curve could be interpreted to represent 100% deoxygenated blood, a situation not representative of a live patient. The dashed curve in the same figure illustrates the overall absorption coefficient as a function of wavelength that leads to the oxygen saturation value of 0.95. Its profile is very similar to that of the 100% oxygenated Hb. The spectral coefficient for deoxygenated Hb, therefore, has only limited effect on the amount of transilluminated radiation. For this reason, the peak shape and the wavelength of its maximum exert only a decreased influence on the amount of transilluminated radiation.

Oxygen saturation, S, is the amount of oxygen in total hemoglobin (THb) calculated as a ratio of the HbO_2 concentration to the total hemoglobin concentration $c_T = c_{OH} + c_{DH}$.

$$S = c_{OH}/c_T = c_{OH}/(c_{OH} + c_{DH}). \tag{1}$$

The lower limit in the range 0.8 to 1.0 in the functional saturation sets the optimistic limit, where an otherwise healthy patient might still have a chance to recover from short-term oxygen deprivation. The latter (1.0) is the value measured for a healthy young man at the peak of his physical abilities. At the critical saturation of 0.9, the HbO_2 concentration contributes 90% to the absorption and only 10% to the Hb concentration.

2.2 *Oxygen Saturation from Measured Transillumination*

Next, we review the principal steps in the theoretical development to derive the oxygen saturation expression. We start with the Beer–Lambert attenuation law. We formulate it for the spectral power incident per unit area of the transilluminated sample. A general sample includes segments other than arterial blood, whose radiometric characteristics do not contribute to the oximetry signal, including skin (twice), fatty layer (possibly twice), flesh, and bone.[55] Other parts contribute to scattering and absorption losses. We assume that one segment of the transilluminated sample includes arterial blood.

$$M(L, \lambda, t) = T_l M_0 \exp\{-L(t)[\mu(\lambda) + \gamma(\lambda)]\} \ [\mathrm{W/cm^2}] \tag{2}$$

Here, the product $T_l = (A_l)(R_l)$ represents the transmission losses, characteristic only of the site where the probe is applied. A_1 is the path-integrated, or total, absorption excluding that ascribed to the hemoglobin component. Similarly, R_l represents the total reflection including that at the boundaries between tissues and upon incidence on the sample. Neither of these terms depends on the degree of the blood oxygenation. The transmission loss term is <1; therefore, an illumination source with high-peak emission is desirable.

Finally, M_0 represents the incident radiation emitted by an illumination source (W/cm^2), while M is the transmitted incidence (W/cm^2). It depends on the thickness of the artery, probe wavelength, λ, and time t. The symbols $\mu(\lambda)$ and $\gamma(\lambda)$ denote the linear coefficients of absorption and scattering, respectively, in cm^{-1}. $L(t)$ is the distance traveled by the trans-illuminated radiation (cm). Its time dependence arises from the blood volumetric changes introduced by the heart pumping function.

The hemoglobin-dependent terms (HbO_2 and Hb) contribute to the beam attenuation, according to their concentration and the specific absorption coefficients at the probe wavelengths.

$$M(L,\lambda,t) = T_l M_0 \exp\{-L(t)[\mu_{OH}(\lambda) + \mu_{DH}(\lambda) + \gamma(\lambda)]\} \ (\mathrm{W/cm^2}) \tag{3}$$

Here, $\mu_{OH}(\lambda)$ and $\mu_{DH}(\lambda)$ denote the absorption coefficients of the HbO_2 and Hb concentrations, respectively. We separate the effects of scattering from the absorption remembering the rule for the addition of exponents: $\exp(a+b) = \exp(a)\exp(b)$

$$M(L,\lambda,t) = T_l \exp\{-[L(t)\gamma(\lambda)]\} M_0 \exp\{-L(t)[\mu_{OH}(\lambda) + \mu_{DH}(\lambda)]\} \ (\mathrm{W/cm^2}). \tag{4}$$

Here, we assume that the degree of oxygen saturation level does not affect the amount of scattering. We denote by T the product of all these coefficients.

$$T(L,\lambda,t) = T_l \exp\{-[L(t)\gamma(\lambda)]\}. \tag{5}$$

The HbO_2 and Hb absorption coefficients $\mu(\lambda)$ are equal to the concentration c in molar units M multiplied by the specific absorption coefficient $\varepsilon(\lambda)$ in cm^{-1} M^{-1}.

$$\mu_{OH}(\lambda) = c_{OH}\varepsilon_{OH}(\lambda) \quad \text{and} \quad \mu_{DH}(\lambda) = c_{DH}\varepsilon_{DH}(\lambda) \ (\mathrm{cm^{-1}}) \tag{6}$$

The HbO_2- and Hb-specific absorption coefficients, $\varepsilon_{OH}(\lambda)$ and $\varepsilon_{DH}(\lambda)$, depend on wavelength; they are known quantities and are graphed in Fig. 1. The HbO_2 and Hb concentrations, c_{OH} and c_{DH}, are independent of wavelength; they are unknown key parameters measured for each saturation determination. First, we substitute Eqs. (5) and (6) into Eq. (3):

$$M(L,\lambda,t) = \mathrm{TM}_0 \exp\{-[c_{OH}\varepsilon_{OH}(\lambda) + c_{DH}\varepsilon_{DH}(\lambda)]L(t)\} \ [\mathrm{W/cm^2}]. \tag{7}$$

We divide both sides of Eq. (7) by the incidence, M_0, and the transmission losses, T. We denote this normalized quantity as $m(L,\lambda,t)$:

$$m(L,\lambda,t) = \exp\{-[c_{OH}\varepsilon_{OH}(\lambda) + c_{DH}\varepsilon_{DH}(\lambda)]L(t)\}. \tag{8}$$

Then, we take the logarithm of the normalized incidence, $m(L,\lambda,t)$:

$$\ln m(L,\lambda,t) = -[c_{OH}\varepsilon_{OH}(\lambda) + c_{DH}\varepsilon_{DH}(\lambda)]L(t). \tag{9}$$

The transillumination measurements are performed at two wavelengths, λ_1 and λ_2. The objective of much of current oximetry research is to determine which two wavelengths (as a minimum) will provide the saturation value with the highest accuracy. After systematic spectral evaluation for any combination of wavelength pairs within the therapeutic window, we found the error in measurement accuracy to be quite pronounced, increasing from 0 to several percent up to 15% for some choices of wavelength pairs. This error interval is nearly the same as the width of the functional saturation range. Within clinical applications, the accuracy of the oxygenation determination is improved by repeated measurements. This area of the administration of patient care offers the possibility of improvement.

We express Eq. (9), evaluated for wavelengths λ_1 and λ_2, in terms of saturation, S, using Eq. (1). We express the product of total hemoglobin concentration c_T with $L(t)$ as $D(t)[= c_T L(t)]$.

$$\ln m_1(D,\lambda,t) = -\{S[\varepsilon_{OH}(\lambda_1) - \varepsilon_{DH}(\lambda_1)] + \varepsilon_{DH}(\lambda_1)\}D(t), \tag{10a}$$

$$\ln m_2(D,\lambda_2,t) = -\{S[\varepsilon_{OH}(\lambda_2) - \varepsilon_{DH}(\lambda_2)] + \varepsilon_{DH}(\lambda_2)\}D(t). \tag{10b}$$

Then, after some manipulation, we find the saturation expression:

$$S(\lambda_1,\lambda_2,m_1,m_2) = \frac{\varepsilon_{DH}(\lambda_1)\ln m_2(D,\lambda_2) - \varepsilon_{DH}(\lambda_2)\ln m_1(D,\lambda_1)}{[\varepsilon_{OH}(\lambda_2) - \varepsilon_{DH}(\lambda_2)]\ln m_1(D,\lambda_1) - [\varepsilon_{OH}(\lambda_1) - \varepsilon_{DH}(\lambda_1)]\ln m_2(D,\lambda_2)}. \tag{11}$$

The oxygen saturation expression S depends on four variables: two chosen wavelengths and two measured transmitted incidences at these wavelengths.

This saturation expression excludes the noise contributions that accompany and degrade most experimental measurements. The noise effects are decreased when the measured signal is maximized. We propose to accomplish this goal by employing (1) probe wavelengths where the absorption is low and (2) illumination sources with high-spectral emission in the low-noise spectral bands.

2.3 *Standard Deviation Versus Probe Wavelengths*

Figure 2 presents the standard deviation of thousands of measured saturation values as a function of the wavelengths λ_1 and

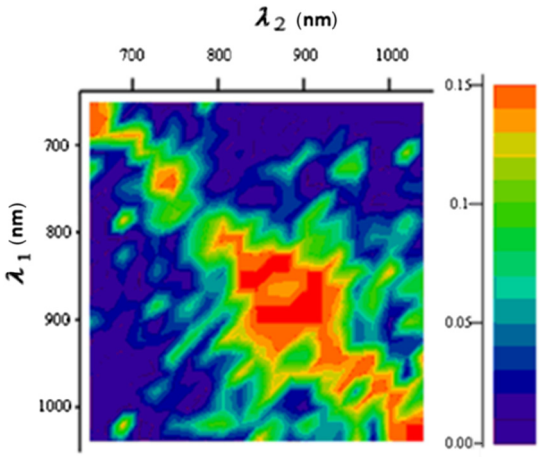

Fig. 2 Standard deviation of saturation measurements as a function of two wavelengths in the therapeutic window. Black (or dark blue) indicates low noise value resulting in enhanced quality of measurements. Only lower left corner and upper right corner appear to be mostly noise-free. The source of transilluminated radiation is white light. A forearm of a lean, healthy man in his mid-30s at rest serves as a transilluminated sample.

λ_2 within the therapeutic window. A forearm of a lean, healthy man in his mid-30s at a state of rest serves as a sample. A white light source is used as the illumination source. A 0.6-nm spectral resolution spectrometer measures the transmitted spectral radiation. We observe that the spectral region defined by $\lambda_1 = -\lambda_2 \pm \Delta\lambda$ is characterized by the error equal to the range of functional saturation. The width of the noise interval $2\Delta\lambda$ increases significantly with wavelength.

Only lower left corner and upper right corner of Fig. 2 appear to be relatively noise-free, in general agreement with previous research. The most favorable intervals identified for a thick transmission sample, such as a forearm, include three regions:

1. $[900\,\text{nm} \le \lambda_1 \le 1000\,\text{nm}]$ and $[650\,\text{nm} \le \lambda_2 \le 720\,\text{nm}]$;
2. $[650\,\text{nm} \le \lambda_1 \le 740\,\text{nm}]$ and $[800\,\text{nm} \le \lambda_2 \le 910\,\text{nm}]$;
3. $[650\,\text{nm} \le \lambda_1 \le 700\,\text{nm}]$ and $[900\,\text{nm} \le \lambda_2 \le 1040\,\text{nm}]$.

Next, we examine the effects of temporal phenomena on the transillumination measurements.

3 Effects of Time-Dependent Breathing on Transillumination Measurements

$L(t)$ in cm is the distance traveled by the transilluminated radiation inside the artery. It is time dependent, because the breathing and cardiac pumping cycles produce expansion in artery volume and accelerate the blood throughput. Figure 3, left, shows the normalized maximum and minimum transillumination as a function of wavelength measured in our laboratory on a thumb of a lean, healthy male in his mid-30s at rest for 30 s. Two curves correspond to the systole (minimum) and the diastole (maximum) periodicity of the heart activity. Figure 3, right, presents the difference between the maximum and the minimum transillumination or the peak-to-peak modulation as a function of wavelength.

The modulation amplitude reaches the peak value at 710 nm, constituting ~3% of the time-independent signal. It decreases to zero for shorter wavelengths and approaches asymptomatically the value of 0.5% (0.005) of the time-independent signal for longer wavelengths, specifically in the spectral band [875 to 980 nm]. Choosing the upper wavelength within this window will ameliorate temporal effects in saturation determination. Also, the choice of two wavelengths (or spectral bands as we discuss later) that have the same value for the average temporal fluctuations is expected to generate saturation values less susceptible to temporal measurement error. Thus, the probing intervals should preferably be located on different sides of the peak of the modulated curve.

3.1 *Absorption Sensitivity to Temporal Noise*

In Fig. 4, we present the time evolution of the transillumination spectral lines through the forearm of a lean, healthy male in his mid-30s in a state of rest. These wavelengths are 660, 767, 811,

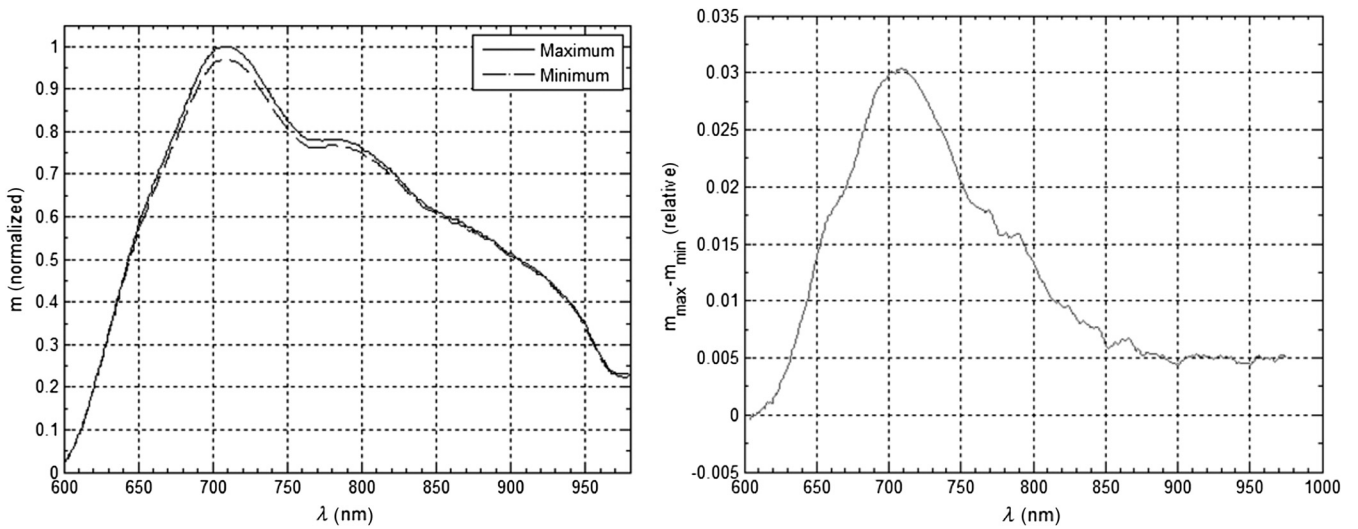

Fig. 3 Measured maximum and minimum transillumination spectra as a function of wavelength arising from the heart activity during the systole (minimum) and the diastole (maximum) cycle. The curves are obtained at 30 s from the measured transillumination spectrum in the therapeutic window through the index finger of a healthy male in his mid-30s at a state of rest. The difference between curves is shown on the expanded scale on the right. The highest difference between the signals is observed around 710 nm. At this wavelength, the modulation reaches 3%.

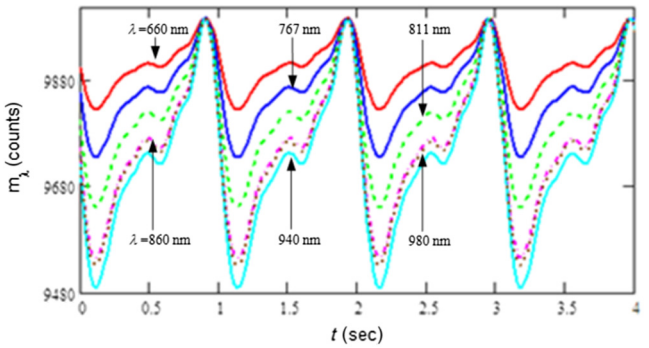

Fig. 4 Transillumination spectra at several wavelengths (660, 767, 811, 860, 940, and 980 nm) as a function of time for a lean, healthy male in his mid-30s measured through forearm at a state of rest. Toward the longer wavelengths of the therapeutic window, we observe an increasingly higher modulation of the transillumination signal. At longer wavelengths still, the modulation decreases again. It is about the same at 860 and 980 nm, achieving the maximum at ~940 nm. The spectral location of the maximum modulation is displaced from that in Fig. 3, due to different pumping force experienced at the different location on the body. Greater volume of blood as a consequence of volume expansion may be responsible for the shift in modulation to longer wavelengths.

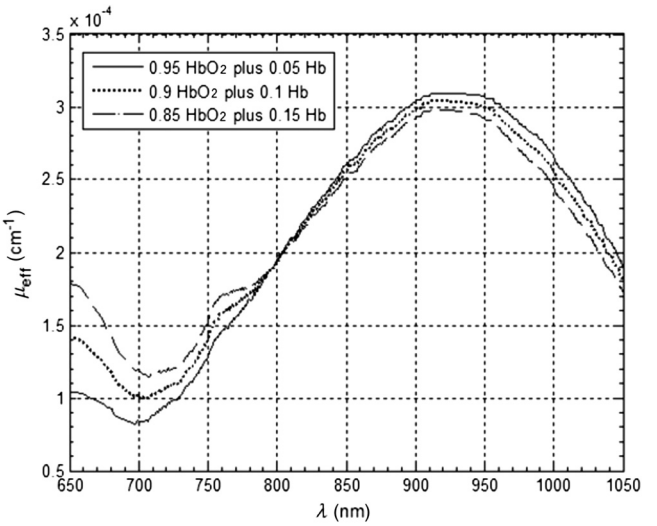

Fig. 5 The effective absorption coefficient as a function of wavelength with the oxy-hemoglobin concentration as a parameter.

860, 940, and 980 nm. Here, we can appreciate the periodic nature of the time-dependent component of the transillumination signal. Their waveform repeats with the periodicity of the heartbeat, allowing for the simultaneous measurement of the heartbeat and the oxygen saturation. Toward the longer wavelengths of the therapeutic window, we observe higher modulation of the transillumination signal. At long NIR wavelengths still within the therapeutic window, the modulation decreases again. It is about the same at 860 and 980 nm, achieving the maximum at about 940 nm.

We remark on an interesting difference between results presented in Figs. 3 and 4, both measured on the same individual, but on different body locations with different tissue thickness. The maximum modulation is detected at a wavelength appreciably shifted toward the longer wavelengths of the therapeutic window for trans-illumination at a forearm. This may be caused by different distance from the heart, along the arterial path, or different arterial thickness $L(t)$.

We measured several transillumination spectra for a number of subjects at distinct body locations of both sexes and a range of statures. We analyzed transillumination signals at different wavelengths and in diverse measurement settings on the index finger, around the nail, on the first phalange, and on the forearm. The periodic shape of the measured signal and its amplitude change to some degree depend on the measurement site even for the same individual, but they always maintain a general saw-tooth waveform.

3.2 *Absorption Sensitivity to* HbO_2 *Concentration for Critical Saturation*

The general equation for the natural logarithm of the normalized transilluminated radiation is given in Eq. (10). The amount of normalized transilluminated radiation, $m(L,\lambda)$, is measured at two wavelengths to determine the saturation and the total hemoglobin concentration, c_T. We denote the factor that multiplies the distance $L(t)$ as the effective absorption coefficient, $\mu_{eff}(\lambda)$.

$$\mu_{\text{eff}}(\lambda) = [S\varepsilon_{\text{OH}}(\lambda) + (1-S)\varepsilon_{\text{DH}}(\lambda)]c_T \ (\text{cm}^{-1}) \qquad (12)$$

The effective absorption coefficient is depicted in Fig. 5 as a function of wavelength for three special cases: (1) the critical mixture of 0.9 HbO_2 and 0.1 Hb giving rise to critical saturation and a small range of values around the critical mixture, (2) 0.95 HbO_2 and 0.05 Hb, and (3) 0.85 HbO_2 and 0.15 Hb.

Upon analyzing the curves in Fig. 5 in more detail, we observe that the effective absorption coefficient is about the same for HbO_2 and Hb concentrations within the functional saturation for the wavelengths in the narrow spectral interval [770 to 820 nm]. The crossover region is shifting toward longer wavelengths with increasing concentration of HbO_2. This means that the transillumination measurements within this spectral interval are not sensitive to the changes in the concentrations of HbO_2. The absorption coefficient for a wavelength in this interval is independent of the HbO_2 concentration within the range of the functional saturation.

Furthermore, on the right of this wavelength interval (820 nm), the effective absorption coefficient increases with increasing HbO_2 concentration. A significant and nearly constant increase in the absorption coefficient of 2 cm^{-1}/mole of HbO_2 concentration may be noted for wavelengths longer than 920 nm. The spectral region beyond 1000 nm is similarly very sensitive to the change in the HbO_2 concentration. Additionally, it has a relatively low absorption coefficient in this spectral interval. These two characteristics make this wavelength (band) highly favorable.

On the short wavelength side of the spectral window [770 to 820 nm], the effective absorption coefficient decreases with increasing HbO_2 concentration. A pronounced and well-defined decrease in the effective absorption coefficient of 6 cm^{-1}/mole of HbO_2 concentration is observed for wavelengths shorter than 720 nm. The spectral region below 720 nm is clearly the most sensitive to the change in HbO_2 concentration in the therapeutic window.

The spectral line at 660 nm corresponds to the first probe wavelength in many commercially available oximeters. According to the idea of maximizing the transmitted signal at the probe wavelengths (and spectral bands), we propose the

probe wavelength at and around 700 nm where the effective absorption attains its minimum value, while maintaining a very high sensitivity to the change in the HbO_2 concentration.

Either the solid-state lasers or the LED illumination sources generate spectral incidence in an interval around the nominal value. Therefore, transilluminated signal must be maximized for the complete spectral interval with greater weight given to the spectral regions with higher radiative emission. The choice of the NIR wavelength is more challenging, requiring the incorporation of an IR source. We next describe the availability of these sources, providing their measured spectral characteristics.

4 NIR LEDs as Illumination Sources

We examine again Fig. 2, presenting the standard deviation of saturation measurements as a function of probe wavelengths, each one running through complete set of wavelengths in the therapeutic window. We observe that the central domain along the diagonal with the probe wavelengths $\lambda_1 = -\lambda_2$, ranging from 780 to 1050 nm, suffers from an unacceptable level of noise. The predominance of noisy measurements in the low-wavelength half of this interval may be explained by the nearly indistinguishable effective absorption coefficient for the HbO_2 concentrations within the range of functional saturation (see Fig. 5). The high-temporal modulation level at and around 940 nm may be responsible for the elevated levels of noise in the upper-wavelength half of this domain.

Three details of Fig. 2, exhibiting very low noise, are featured in Fig. 6. The lower left corner and the upper right corner in Fig. 2 may be suitable for probing and illuminating with an extended spectral source. The most favorable spectral intervals for oximetry measurements are identified for a thick transmission sample, such as a forearm. Upon further examination, we identify some small wiggly regions of elevated standard deviation. There appears a totally error-free wavelength region within spectral limits: $[935\ \text{nm} \le \lambda_1 \le 1000\ \text{nm}]$ and $[660\ \text{nm} \le \lambda_2 \le 710\ \text{nm}]$. The two-dimensional standard deviation is not symmetrical in two wavelengths. This is attributed to measurement errors and temporal noise.

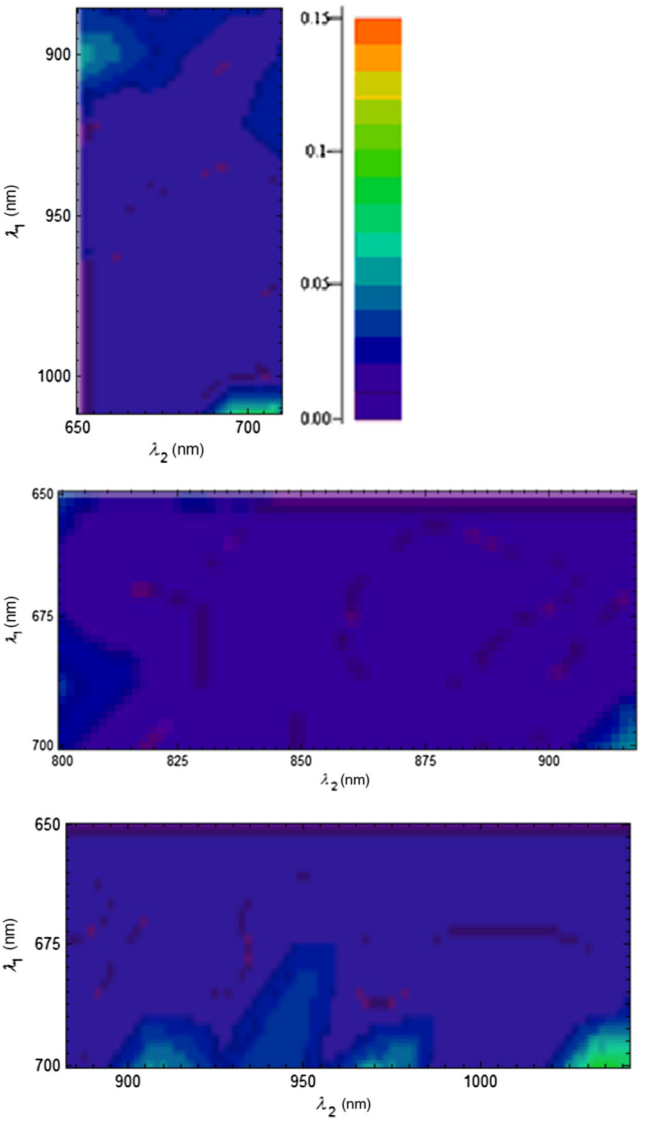

Fig. 6 Three domains with very low-noise levels may be identified from Fig. 3. (a) Lower left corner: λ_1 ranges from 900 to 1000 nm and λ_2 increases from 650 to 750 nm. (b) Upper right corner: λ_1 ranges from 650 to 700 nm and λ_2 increases from 900 to 1000 nm. (c) Upper right region: λ_1 ranges from 650 to 700 nm and λ_2 increases from 800 to 900 nm.

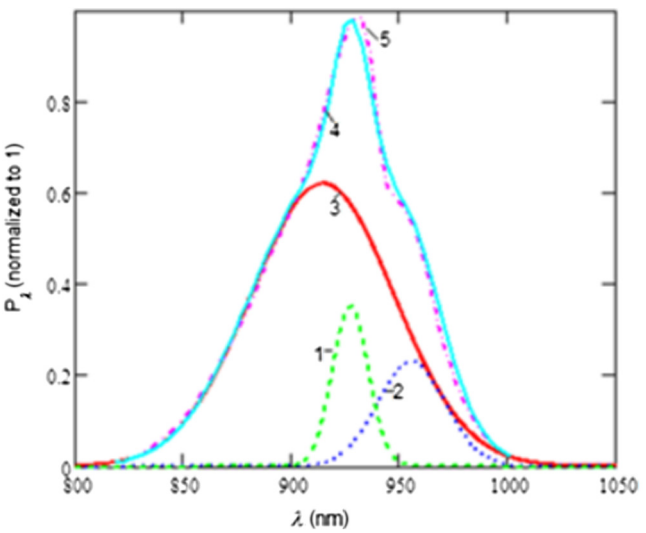

Fig. 7 Measured spectral distribution of five NIR light emission diodes (LEDs) with peak emissions between 930 and 970 nm. Table 1 summarizes the measured spectral parameters.

Table 1 Measured spectral characteristics of light emission diodes (LEDs). The subscript "hm" denotes full-width-at-half-maximum, "fw" is full width, and p refers to the wavelength at peak emission.

No.	λ_p (nm)	$M(\lambda_p)$ (normalized)	$\Delta\lambda_{hm}$ (nm)	$\Delta\lambda_{fw}$ (nm)
1	930	0.35	25	50
2	970	0.24	40	90
3	920	0.6	70	420
4	925	1.0	70	400
5	930	1.0	70	400

Figure 7 presents measured spectral emission of five NIR LEDs peaking at 915, 920, 925, 930, and 960 nm. Experimental setup to measure the spectral distribution of NIR LEDs includes the LED under test, an integrating sphere, an optical fiber, a high-spectral-resolution spectrometer, and a PC to process the data and display the results.

Table 1 includes the list of measured spectral parameters: full spectral width of the LED source, full width of the spectral source at half maximum, and the wavelength of peak emission. The range of relative peak emissions spans a factor of 4.

5 Conclusions

We proposed a new evaluation method for the selection of optimal probe wavelengths in oxygen saturation-measuring device for application to a thick sample. It is based on the blood absorption characteristics of oxygenated hemoglobin at the critical oxygen saturation of 0.9.

We determined the spectral sensitivity of the absorption coefficient to the concentration of oxy-hemoglobin. We found that there is an interval approximately at the center of the therapeutic interval, where the effective absorption coefficient does not change with the concentration of oxygenated hemoglobin for the functional saturation interval. Thus, a probe wavelength in this spectral interval results in saturation determination with low reliability.

Furthermore, we observed that the amplitude of time-dependent portion of the transillumination signal actually changes with the location on the body. We ascribe the increase in signal with longer wavelengths to the proximity to heart, and higher blood flow before the bifurcation of arteries into small veins. On the same individual, we observed a shift from the peak modulation at 710 to 940 nm, when the site changed from the index finger to a forearm.

The most favorable interval for interrogating a thick transmission sample, such as a forearm, is $[900\ \text{nm} \le \lambda_1 \le 1000\ \text{nm}]$ and $[650\ \text{nm} \le \lambda_2 \le 720\ \text{nm}]$. The LED with peak power emission at wavelength of 930 nm provides ample illumination power for this spectral region. Here, the effective absorption coefficient is strongly dependent on the oxygenated hemoglobin concentration.

Acknowledgments

The authors acknowledge CONACyT, the Mexican National Science Foundation, which provided funding for this research.

References

1. A. N. Yaroslavsky et al., "Optics of blood," in *Handbook of Optical Biomedical Diagnostics*, V. V. Tuchin, Ed., pp. 169–216, SPIE Press, Bellingham, Washington (2002).
2. H. Liu et al., "Determination of optical properties and blood oxygenation in tissue continuous NIR light," *Phys. Med. Biol.* **40**(11), 1983–1993 (1995).
3. A. Cysewska-Sobusiak, "One-dimensional representation of light-tissue interaction for application in noninvasive oximetry," *Opt. Eng.* **36**(4), 1225–1233 (1997).
4. J. Shao et al., "Theoretical and experimental studies on linear and nonlinear algorithms for the measurement of muscle oxygenation using continuous-wave near-infrared spectroscopy," *Opt. Eng.* **40**(10), 2293–2301 (2001).
5. J. P. Culver et al., "Volumetric diffuse optical tomography of brain activity," *Opt. Lett.* **28**(21), 2061–2063 (2003).
6. J. H. Choi et al., "Noninvasive determination of the optical properties of adult brain: near-infrared spectroscopy approach," *J. Biomed. Opt.* **9**(1), 221–229 (2004).
7. E. Gratton et al., "Measurement of brain activity by near-infrared light," *J. Biomed. Opt.* **10**(1), 8–13 (2005).
8. P. Vacas-Jacques, M. Strojnik, and G. Paez, "Forward-calculated analytical interferograms in pass-through photon-based biomedical transillumination," *J. Opt. Soc. Am. A* **26**(3), 602–612 (2009).
9. P. Vacas-Jacques, G. Paez, and M. Strojnik, "Pass-through photon-based biomedical transillumination," *J. Biomed. Opt.* **13**(4), 041307 (2008).
10. S. Wray et al., "Characterization of the near infrared absorption spectra of cytochrome aa3 and hemoglobin for the non invasive monitoring of cerebral oxygenation," *Biochim. Biophys. Acta* **933**(1), 184–192 (1988).
11. M. Nitzan et al., "Measurement of oxygen saturation in venous blood by dynamic near infrared spectroscopy," *J. Biomed. Opt.* **5**(2), 155–162 (2000).
12. M. J. Hayes and P. R. Smith, "A new method for pulse oximetry possessing inherent insensitivity to artifact," *IEEE Trans. Biomed. Eng.* **48**(4), 452–461 (2001).
13. S. Fantini and M. A. Franceschini, "Frequency-domain techniques for tissue spectroscopy and imaging," in *Handbook of Optical Biomedical Diagnostics*, V. V. Tuchin, Ed., pp. 405–453, SPIE Press, Bellingham, Washington (2002).
14. M. T. Petterson, V. L. Begnoche, and J. M. Graybeal, "The effect of motion on pulse oximetry and its clinical significance," *Anesth. Analog.* **105**(Online Suppl.), S78–S84 (2007).
15. O. Desebbe and M. Cannesson, "Using ventilation induced plethysmographic variations to optimize patient fluid status," *Curr. Opin. Anaesthesiol.* **21**(6), 772–778 (2008).
16. B. W. Pogue and M. S. Patterson, "Review of tissue simulating phantoms for optical spectroscopy, imaging and dosimetry," *J. Biomed. Opt.* **11**(4), 1–16 (2006).
17. J. d Mobley and T. Vo-Dinh, "Light-tissue interactions," in *Biomedical Photonics Handbook*, T. Vo-Dinh, Ed., pp. 2-1–2-71, CRC Press, New York (2003).
18. M. Niwayama et al., "Quantitative measurement of muscle hemoglobin oxygenation using near-infrared spectroscopy with correction of the influence of a subcutaneous fat layer," *Rev. Sci. Instrum.* **71**(12), 4571–4575 (2000).
19. R. N. Pittman, "In vivo photometric analysis of hemoglobin," *Ann. Biomed. Eng.* **14**(2), 119–137 (1986).
20. P. D. Mannheimer et al., "Wavelength selection for low saturation pulse oximetry," *IEEE Trans. Biomed. Eng.* **44**(3), 148–58 (1997).
21. M. Nitzan and E. Shlomo, "Three-wavelength technique for the measurement of oxygen saturation in arterial blood and in venous blood," *J. Biomed. Opt.* **14**(2), 1–6 (2009).
22. M. Rothmaier et al., "Photonic textiles for pulse oximetry," *Opt. Express* **16**(17), 12973–12986 (2008).
23. S. J. Barker et al., "Measurements or carboxyhemoglobin and methemoglobin by pulse oximetry: a human volunteer study," *Anesthesiology* **105**(5), 892–897 (2006).
24. C. Baker, "Pulse oximeter with parallel saturation calculation modules," U. S. Patent No. 20050124871 (2005).
25. D. J. Sebald, "Motivation of pulse oximetry," in *Design of Pulse Oximeters*, J. G. Webster, Ed., p. 15, IOP Publishing, Bristol, UK (1997).
26. C. D. Kurth and W. Thayer, "A multi-wavelength frequency-domain near-infrared cerebral oximeter," *Phys. Med. Biol.* **44**(3), 727–740 (1999).
27. T. Aoyagi and K. Miyasaka, "Pulse oximetry: its invention, contribution to medicine and future tasks," *Anesth. Analg.* **94**(Suppl. 1), S1–S3 (2002).
28. T. Aoyagi, "Pulse oximetry: its invention, theory, and future," *J. Anesth.* **17**(4), 259–266 (2003).
29. T. Aoyagi et al., "Multi-wavelength pulse oximetry: theory for the future," *Anesth. Analg.* **105**(6S_Suppl.), S53–S58 (2007).
30. M. Cannesson and P. Talke, "Recent advances in pulse oximetry," *Med. Rep.* **1**, 66 (2009).
31. M. H. Smith, "Optimum wavelength combinations for retinal vessel oximetry," *Appl. Opt.* **38**(1), 258–267 (1999).
32. L. A. Nelson et al., "Development and validation of a multi-wavelength spatial domain near-infrared oximeter to detect cerebral hypoxia-ischemia," *J. Biomed. Opt.* **11**(6), 064022 (2006).
33. T. K. Aldrich et al., "Length-normalized pulse photoplethysmography: a noninvasive method to measure blood hemoglobin," *Ann. Biomed. Eng.* **30**(10), 1291–1298 (2002).

34. K. H. Shelley, "Photoplethysmography: beyond the calculation of arterial oxygen saturation and heart rate," *Anesth. Analg.* **105**(6S_Suppl.), S31–S36 (2007).
35. K. Humphreys, T. Ward, and C. Markham, "Noncontact simultaneous dual wavelength photoplethysmography: a further step toward noncontact pulse oximetry," *Rev. Sci. Instrum.* **78**(4), 1–6 (2007).
36. N. Ignjatovic et al., "Diagnostic importance of pulse oximetry in the determination of the stage of chronic arterial insufficiency of lower extremities," *Srp. Arh. Celok. Lek.* **138**(5–6), 300–304 (2010).
37. C. D. Kurth and W. Thayer, "A multi-wavelength frequency-domain near-infrared cerebral oximeter," *Phys. Med. Biol.* **44**(3), 727–740 (1999).
38. S. Fantini et al., "Non-invasive optical mapping of the piglet brain in real time," *Opt. Express* **4**(8), 308–314 (1999).
39. J. W. Salyer, "Neonatal and pediatric pulse oximetry," *Respir. Care* **48**(4), 386–396 (2003).
40. B. J. Tromberg et al., "Assessing the future of diffuse optical imaging technologies for breast cancer management," *Med. Phys.* **35**(6), 2443–2451 (2008).
41. J. P. Phillips et al., "An esophageal pulse oximetry system utilizing a fiber-optic probe," *J. Phys. Conf. Ser.* **178**(1), 012021 (2009).
42. S. M. Lopez-Silva, M. L. Dotor-Castilla, and J. P. Silveira-Martin, "Near-infrared transmittance pulse oximetry with laser diodes," *J. Biomed. Opt.* **8**(3), 525–533 (2003).
43. J. Allen, "Photoplethysmography and its application in clinical physiological measurement," *Physiol. Meas.* **28**, R1–R39 (2007).
44. W. Verkruysse, L. O. Svaasand, and J. S. Nelson, "Remote plethysmographic imaging using ambient light," *Opt. Express* **16**(26), 21434–21445 (2008).
45. G. Cennini et al., "Heart rate monitoring via remote photoplethysmography with motion artifacts reduction," *Opt. Express* **18**(5), 4867–4875 (2010).
46. F. P. Wieringa et al., "In vitro demonstration of an SpO_2-camera," *Comput. Cardiol.* **34**, 749–751 (2007).
47. S. Hu et al., "Development of effective photoplethysmographic measurement techniques: from contact to non-contact and from point to imaging," in *Proc. IEEE Conf. Engineering in Medicine and Biology*, pp. 6550–6553, Institute of Electrical and Electronics Engineers, New York (2009).
48. T. Li et al., "Simultaneous measurement of deep tissue blood flow and oxygenation using noncontact diffuse correlation spectroscopy flow-oximeter," *Sci. Rep.* **3**, 01358 (2013).
49. A. A. Kamshilin et al., "Photoplethysmographic imaging of high spatial resolution," *Biomed. Opt. Express* **2**(4), 996–1006 (2011).
50. J. Spigulis, "Biophotonic technologies for non-invasive assessment of skin condition and blood microcirculation," *Latv. J. Phys. Tech. Sci.* **49**(5), 63–80 (2012).
51. T. D. O'Sullivan et al., "Diffuse optical imaging using spatially and temporally modulated light," *J. Biomed. Opt.* **17**(7), 071311 (2012).
52. J. A. Rice, *Mathematical Statistics and Data Analysis*, 2nd ed., Duxburry Press, Pacific Grove, California (1995).
53. C. Vasquez-Jaccaud, G. Paez, and M. Strojnik, "Wavelength selection method with standard deviation: application to pulse oximetry," *Ann. Biomed. Eng.* **39**(7), 1994–2009 (2011).
54. M. Strojnik and G. Paez, "Radiometry," in *Handbook of Optical Engineering*, D. Malacara and B. Thompson, Eds., Marcel Dekker, New York, pp. 649–700 (2001).
55. T. Lister, P. A. Wright, and P. H. Chappell, "Optical properties of human skin," *J. Biomed. Opt.* **17**(9), 090901 (2012).